Inorg. Chem. **2007**, *46*, 11094–11105

Facilitated Hydride Binding in an Fe–Fe Hydrogenase Active–Site Biomimic Revealed by X-ray Absorption Spectroscopy and DFT Calculations

Simone Löscher,[†] Lennart Schwartz,[‡] Matthias Stein,[§] Sascha Ott,*[,‡] and Michael Haumann*[,†]

Freie Universität Berlin, Institut für Experimentalphysik, Arnimallee 14, 14195 Berlin, Germany, Uppsala University, Department of Photochemistry and Molecular Science, Box 523, 75120 Uppsala, Sweden, EML Research gGmbH, Schloss-Wolfbrunnenweg 33, 69118 Heidelberg, Germany

Received June 26, 2007

Iron-only hydrogenases are high-efficiency biocatalysts for the synthesis and cleavage of molecular hydrogen. Their active site is a diiron center, which carries CO and CN ligands. Remarkably, the two iron atoms likely are connected by a non-protein azadithiolate (adt = S–CH_2–NH–CH_2–S). To dwell on the role of the adt in H_2 catalysis, a specific biomimetic diiron compound, **1** = [Fe_2(μ-adt-CH_2–Ph)(CO)$_4$(PMe_3)$_2$], with unprecedented positive reduction potential, has been synthesized and crystallized previously. It comprises two protonation sites, the *N*-benzyl-adt nitrogen that can hold a proton (H) and the Fe–Fe bond that will formally carry a hydride (Hy). We investigated changes in the solution structure of **1** in its four different protonation states (**1′**, [1H]$^+$, [1HHy]$^{2+}$, and [1Hy]$^+$) by X-ray absorption spectroscopy at the iron K-edge. EXAFS reveals that already protonation at the adt nitrogen atom causes a change of the ligand geometry involving a significant lengthening of the Fe–Fe distance and CO and PMe_3 repositioning, respectively, thereby facilitating the subsequent binding of a bridging hydride. Hydride binding clearly is discernible in the XANES spectra of [1HHy]$^{2+}$ and [1Hy]$^+$. DFT calculations are in excellent agreement with the experimentally derived structural parameters and provide complementary insights into the electronic structure of the four protonation states. In the iron-only hydrogenases, protonation of the putative adt ligand may cause the bridging CO to move to a terminal position, thereby preparing the active site for hydride binding en route to H_2 formation.

Introduction

The iron-only or Fe−Fe hydrogenases (iron-only H_2ases), abundant in strictly anaerobic bacteria,[1] are high-efficiency biological catalysts for the cleavage of molecular hydrogen and for proton reduction, to yield H_2 with remarkably high turnover rates of up to 6×10^3 s^{-1}.[2] These enzymes are of primary interest in research on future energy technology applications.[3,4] However, today's usefulness of iron-only H_2-ases in biotechnological devices is limited by their irreversible inactivation by O_2.[5] Progress in the understanding of the active-site structure comes from recent crystallographic work on two iron-only H_2ases.[6−9] Biomimetic synthetic chemistry is a powerful tool to clarify the requirements of

* To whom correspondence should be addressed. E-mail: haumann@physik.fu-berlin.de, Tel.: +49 30 8385 6101, Fax: +49 30 8385 6299 (M.H.); Email: sascha.ott@fotomol.uu.se, Fax.: ++46 18 471 6844 (S.O.).
† Freie Universität Berlin.
‡ Uppsala University.
§ EML Research gGmbH.

(1) Vignais, P. M.; Colbeau, A. Molecular biology of microbial hydrogenases. *Curr. Issues Mol. Biol.* **2004**, *6*, 159−188.
(2) Adams, M. W. W. The Structure and Mechanism of Iron-Hydrogenases. *Biochim. Biophys. Acta* **1990**, *1020*, 115−145.
(3) Mertens, R.; Liese, A. Biotechnological applications of hydrogenases. *Curr. Opin. Biotechnol.* **2004**, *15*, 343−348.
(4) Das, D.; Dutta, T.; Nath, K.; Kotay, S. M.; Das, A. K.; Vetiroglu, T. N. Role of Fe-Hydrogenases in Biological Hydrogen Production. *Curr. Sci.* **2006**, *90*, 1627−1637.
(5) Vincent, K. A.; Perkin, A.; Lenz, O.; Albracht, S. P.; Fontecilla-Camps, J. C.; Cammack, R.; Friedrich, B.; Armstrong, F. A. Electrochemical Definitions of O_2 Sensitivity and Oxidative Inactivation in Hydrogenases. *J. Am. Chem. Soc.* **2005**, *127*, 18179-18189.
(6) Peters, J. W.; Lanzilotta, W. N.; Lemon, B.; Seefeldt, L. C. X-ray Crystal Structure of the Fe-Only Hydrogenase (CpI) from *Clostridium pasteurianum* to 1.8 Å Resolution. *Science* **1998**, *282*, 1853−1858.
(7) Nicolet, Y.; Piras, C.; Legrand, P.; Hatchikian, C. E.; Fontecilla-Camps, J. C. *Desulfovibrio desulfuricans* Iron Hydrogenase: The Structure Shows Unusual Coordination to an Active Site Fe Binuclear Center. *Struct. Fold. Des.* **1999**, *7*, 13−23.

10.1021/ic701255p CCC: $37.00
Published on Web 11/28/2007

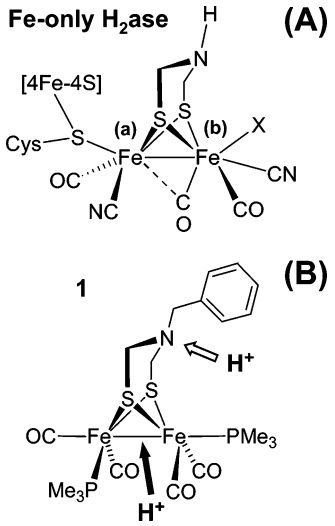

Figure 1. (A) Proposed structure on the basis of crystallographic data of the active site of H_2 conversion, the $[2Fe]_H$-cluster, in the Fe−Fe hydrogenases.[7−9] Ligand X possibly is a water species in the aerobically isolated protein and is absent or replaced by a hydrogen species in the reduced state of the enzyme. The two iron atoms here are denoted as (a) and (b). (B) Schematic drawing of **1**.[32] Its two protonation sites are indicated by arrows.

H_2 catalysis and may lead to effective non-platinum catalysts for the production of H_2 as a fuel in the future.[10]

The active site of iron-only H_2ases commonly is denoted as the H-cluster (part A of Figure 1). It consists of an unusual Fe−Fe unit, $(2Fe)_H$, poised in a low-valence state possibly containing iron(I),[11,12] which carries three CO and two CN ligands[13] and is cysteine-linked to a [4Fe-4S] cluster.[6,7] In the available crystal structures,[6−9] two iron-bridging non-cysteine sulfur atoms have been resolved, and, in addition, there was evidence for a non-protein molecule providing these sulfurs. Various lines of evidence suggested that this molecule is a unique azadithiolate ligand (adt = $S-CH_2-NH-CH_2-S$).[9,14] The nitrogen atom of the adt provides a basic site for protonation according to theoretical investigations[15] and may be connected by a proton channel to the surface of the enzyme.[6] Because proton reduction follows an ionic mechanism,[16] transiently a proton (H^+) may be located at the nitrogen atom of the adt and a hydride (H^-) at a terminal position on iron (i.e., at position X in part A of Figure 1).[9,17] However, computational studies suggested that a hydride bound in a bridging position between the two iron atoms also may be a viable intermediate in catalysis.[18,19] The latter situation is realized in the functionally related Ni−Fe hydrogenases,[20,21] where a Ni−Fe bridging hydride is firmly established in some cases.[22,23] The crystallographic data suggested that the CO group bound in an Fe−Fe bridging position in oxidized iron-only H_2ase (part A of Figure 1) is moved to a terminal position upon the reduction of the enzyme.[7−9] Such structural changes possibly are crucial for hydride binding, but their mechanism is barely understood.

Synthetic model compounds, which reproduce key structural features of the diiron unit of the active site of iron-only H_2ases, have been studied extensively to derive information on the mechanism and standards to assign spectroscopic signatures of the enzymes and to guide the design of novel H_2 catalysts. The $(2Fe)_H$ unit of the enzymes resembles classic $[Fe_2(\mu\text{-}SR)_2(CO)_6]$ derivatives, which have been known for long[24] and may form even under abiotic conditions.[25] Accordingly, the $(2Fe)_H$ might have been incorporated into iron-only H_2ase ancestors as a preformed unit.[7,26,27] A substantial variety of model compounds for the

(8) Lemon, B. J.; Peters, J. W. Binding of Exogenously Added Carbon Monoxide at the Active Site of the Iron-Only Hydrogenase (CpI) from *Clostridium pasteurianum*. *Biochemistry* **1999**, *38*, 12969−12973.
(9) Nicolet, Y.; de Lacey, A. L.; Vernede, X.; Fernandez, V. M.; Hatchikian, E. C.; Fontecilla-Camps, J. C. Crystallographic and FTIR Spectroscopic Evidence of Changes in Fe Coordination upon Reduction of the Active Site of the Fe-Only Hydrogenase from *Desulfovibrio desulfuricans*. *J. Am. Chem. Soc.* **2001**, *123*, 1596−1601.
(10) Evans, D. J.; Pickett, C. J. Chemistry and the Hydrogenases. *Chem. Soc. Rev.* **2003**, *32*, 268−275.
(11) Pereira, A. S.; Tavares, P.; Moura, I.; Moura, J. J.; Huynh, B. H. Mössbauer Characterization of the Iron-Sulfur Centers in *Desulfovibrio vulgaris* Hydrogenase. *J. Am. Chem. Soc.* **2001**, *123*, 2771−2782.
(12) Lyon, E. J.; Georgakaki, I. P.; Reibenspies, J. H.; Darensbourg, M. Y. Coordination Sphere Flexibility of Active-Site Models for Fe-Only Hydrogenase: Studies in Intra- and Intermolecular Diatomic Ligand Exchange. *J. Am. Chem. Soc.* **2001**, *123*, 3268−3278.
(13) Pierik, A. J.; Hulstein, M.; Hagen, W. R.; Albracht, S. P. J. A Low-Spin Iron with CN and CO as Intrinsic Ligands Forms the Core of the Active Site in [Fe]-Hydrogenases. *Eur. J. Biochem.* **1998**, *258*, 572−578.
(14) Nicolet, Y.; Lemon, B. J.; Fontecilla-Camps, J. C.; Peters, J. W. A Novel FeS Cluster in Fe-Only Hydrogenases. *Trends Biochem. Sci.* **2000**, *25*, 138−143.
(15) Fan, H. J.; Hall, M. B. A Capable Bridging Ligand for Fe-Only Hydrogenase: Density Functional Calculations of a Low-Energy Route for Heterolytic Cleavage and Formation of Dihydrogen. *J. Am. Chem. Soc.* 2001, *123*, 3828−3829.
(16) Kubas, G. J. *Metal Dihydrogen and σ-Bond Complexes*; Kluwer Academic Publishers: New York, 2001.
(17) Liu, Z. P.; Hu, P. A. Density Functional Theory Study on the Active Center of Fe-Only Hydrogenases: Characterization and Electronic Structure of the Redox States. *J. Am. Chem. Soc.* **2002**, *124*, 5175−5182.
(18) Bruschi, M.; Fantucci, P.; De Gioia, L. Density Functional Theory Investigations of the Active Site of [Fe]-Hydrogenases: Effects of Redox State and Ligand Characteristics on Structural, Electronic, and Reactivity Properties of Complexes Related to the $[2Fe]_H$ Subcluster. *Inorg. Chem.* **2003**, *42*, 4773−4781.
(19) Zhou, T.; Mo, Y.; Zhou, Z.; Tsai, K. Density Functional Study on Dihydrogen Activation at the H Cluster in Fe-Only Hydrogenases. *Inorg. Chem.* **2005**, *44*, 4941−4946.
(20) Fontecilla-Camps, J. C.; Frey, M.; Garcin, E.; Hatchikian, C.; Montet, Y.; Piras, C.; Vernede, X.; Volbeda, A. Hydrogenase: A Hydrogen-Metabolizing Enzyme. What Do the Crystal Structures Tell Us About Its Mode of Action? *Biochimie* **1997**, *79*, 661−666.
(21) Cammack, R.; Robson, R.; Frey, M. Eds, Hydrogen as a Fuel: Learning from Nature. Taylor & Francis: London, U.K., 1997.
(22) Foerster, S.; van Gastel, M.; Brecht, M.; Lubitz, W. An Orientation-Selected ENDOR and HYSCORE Study of the Ni-C Active State of *Desulfovibrio vulgaris* Miyazaki F Hydrogenase. *J. Biol. Inorg. Chem.* **2005**, *10*, 51−62.
(23) Brecht, M.; Van Gastel, M.; Buhrke, T.; Friedrich, B.; Lubitz, W. Direct Detection of a Hydrogen Ligand in the [NiFe] Center of the Regulatory H_2-Sensing Hydrogenase from *Ralstonia eutropha* in its Reduced State by HYSCORE and ENDOR Spectroscopy. *J. Am. Chem. Soc.* **2003**, *125*, 13075−13083.
(24) Reihlen, H.; von Friedolsheim, A.; Oswald, W. Nitric Oxide and Carbon Monoxide Compounds of Apparently Univalent Iron and Nickel. *J. Liebigs Ann. Chem.* **1928**, *465*, 72−96.
(25) Cody, G. D.; Boctor, N. Z.; Filley, T. R.; Hazen, R. M.; Scott, J. H.; Sharma, A.; Yoder, H. S., Jr. Primordial Carbonylated Iron-Sulfur Compounds and the Synthesis of Pyruvate. *Science* **2000**, *289*, 1337−1340.
(26) Tard, C.; Ibrahim, S. K.; Bruschi, M.; De Gioia, L.; Davies, S. C.; Yang, X.; Wang, L. S.; Sawers, G.; Pickett, C. J. Synthesis of the H-Cluster Framework of Iron-Only Hydrogenase. *Nature* **2005**, *433*, 610−613.
(27) Peters, J. W.; Szilagvi, R. K.; Naumov, A.; Douglas, T. A Radical Solution for the Biosynthesis of the H-Cluster of Hydrogenase. *FEBS Lett.* **2006**, *580*, 363−367.

$(2Fe)_H$ entity has been synthesized and characterized in the last decades (for a comprehensive overview see ref 28). To increase the similarity with the native active site, CO ligands have been replaced by CN^- ligands (e.g., refs 10, 12, and 28−30 and references therein) or phosphorus-containing groups (e.g., refs 31 and 32) have been incorporated at the iron centers. Such substitutions raise the electron density at the iron atoms to facilitate hydride binding. Tempted by the crystal structures of the enzymes[6−9] that are now believed to show adt bridging of the iron atoms, model compounds have been introduced recently, which include an adt derivative.[28,32−35] The adt may play an important role in heterolytic H_2 conversion.[9,15]

Previously, the synthesis and crystallographic structure of a particular biomimetic compound (**1** = $[Fe_2(\mu\text{-}SCH_2N(CH_2\text{-}Ph)CH_2S(CO)_4(PMe_3)_2]$, Ph = phenyl, Me = methyl) has been reported,[32] which carries both an electron-donating phosphine ligand at each iron atom and an adt derivative bridging the two iron centers (part B of Figure 1). IR and NMR spectroscopy have established that this compound stably exists in four protonation states, as induced by the addition of different acids to acetonitrile solutions, namely in the unprotonated form **1′**, as $\mathbf{[1H]^+}$ protonated at the nitrogen atom of the adt, as $\mathbf{[1HHy]^{2+}}$ protonated at the adt and at the Fe−Fe bond, formally yielding a hydride in the bridging position, and as $\mathbf{[1Hy]^+}$ solely possessing the hydride.[32] In **1**,[32] and in the corresponding hexacarbonyl compound,[35] the evolution of H_2 occurred under comparably moderate reducing, electrochemical conditions.

In the solid state, the two PMe_3 ligands in **1** show a mixed basal/apical arrangement.[32] However, ^1H and ^{31}P NMR data have revealed that an isomer, in which both phosphine ligands occupy basal positions, is predominant in solution at room temperature.[41] Even subtle changes in the coordination geometry around the iron atoms are anticipated to be relevant for the mechanism of H_2 catalysis because they alter the electronic properties of the complex, for example, orbital hybridization and occupancy, covalency of the iron-ligand bonds, extent of π-backbonding into the CO/CN ligands, charge density at the iron atoms, and sterical accessibility of the Fe−Fe bond. These properties are expected to influence protonation states and hydride-binding equilibria. Consequently, as benchmarks, for example, for quantum-chemical calculations using DFT[36,37] on the rates and routes of H_2 generation in comparison to the situation in the iron-only H_2ases, atomic-detail information on the solution structure of **1** in its four protonation states is required.

Hydrogen-splitting Ni−Fe H_2ases, hydrogen-generating iron-only H_2ases, and inorganic model complexes have been the subject of various computational studies (for review, see refs 38 and 39 and references therein). For example, Bruschi et al.[40] have investigated the movement of a CO ligand from a semibridging to a terminal position for Fe−Fe active-site models and found that the bridging μ-CO binding is favored by about 6−23 kJ mol^{-1} over the terminal coordination, depending on the iron oxidation state and ligand environment. DFT calculations previously have been used to validate the assignment of the molecular configuration of intermediates of adt-bridged Fe−Fe complexes.[41]

In the present investigation, an element-specific technique providing atomic resolution, namely X-ray absorption spectroscopy (XAS)[42−44] at the iron K-edge, is employed to investigate changes in the Fe−Fe and iron-ligand distances by multiple-scattering EXAFS analysis and changes in the coordination geometry by ab initio XANES simulations in the four different protonation states of **1** in acetonitrile solution. DFT calculations yielded complementary information on the electronic structure of the complex and on the energetic restraints of the uncovered structural rearrangements. It is proposed that protonation of the *N*-adt moiety and resulting structural changes may be of relevance also for the mechanism of H_2 production in the iron-only H_2-ases.

(28) Rauchfuss, T. B. Research on Soluble Metal Sulfides: From Polysulfido Complexes to Functional Models for the Hydrogenases. *Inorg. Chem.* **2004**, *43*, 14−26.

(29) Boyke, C. A.; van der Vlugt, J. L.; Rauchfuss, T. B.; Wilson, S. R.; Zampella, G.; De Gioia, L. Diferrous Cyanides as Models for the Fe-Only Hydrogenases. *J Am Chem Soc.* **2005**, *127*, 11010−11018.

(30) Darensbourg, M. Y.; Lyon, E. J.; Zhao, X.; Georgakaki, I. P. The Organometallic Active Site of [Fe]Hydrogenase: Models and Entatic States. *Proc. Natl. Acad. Sci. U.S.A.* **2003**, *100*, 3683−3688.

(31) Van der Vlugt, J. L.; Rauchfuss, T. B.; Wilson, S. R. Electron-Rich Diferrous-Phosphane-Thiolates Relevant to Fe-Only Hydrogenase: Is Cyanide "Nature's Trimethylphosphane"? *Chem.−Eur. J.* **2005**, *12*, 90−98.

(32) Schwartz, L.; Eilers, G.; Eriksson, L.; Gogoll, A.; Lomoth, R.; Ott, S. Iron Hydrogenase Active Site Mimic Holding a Proton and a Hydride. *Chem. Commun.* **2006**, 520−522.

(33) Lawrence, J. D.; Li, H.; Rauchfuss, T. B.; Benard, M.; Rohmer, M. M. Diiron Azadithiolates as Models for the Iron-Only Hydrogenase Active Site: Synthesis, Structure, and Stereoelectronics. *Angew Chem.* **2001**, *40*, 1768−1771.

(34) Zhao, Z.; Georgakaki, I. P.; Miller, M. L.; Meija-Rodriguez, R.; Chiang, C-Y.; Darensbourg, M. Y. Catalysis of H_2/D_2 Scrambling and Other H/D Exchange Processes by [Fe]-Hydrogenase Model Complexes. *Inorg. Chem.* **2002**, *41*, 3917−3928.

(35) Ott, S.; Kritikos, M.; Akermark, B.; Sun, L.; Lomoth, R. A Biomimetic Pathway for Hydrogen Evolution from a Model of the Iron Hydrogenase Active Site. *Angew Chem.* **2004**, *43*, 1006−1009.

(36) Parr, R. G.; Weitao, Y. *Density Functional Theory of Atoms and Molecules*; Oxford University Press: New York, 1989.

(37) Koch, W.; Holthausen, M. C. A. *Chemist's Guide to Density Functional Theory*; Wiley-VCH: Weinheim, Germany, 2002.

(38) Stein, M.; Lubitz, W. Quantum Chemical Calculations of Ni-Fe Hydrogenases. *Curr. Opin. Chem. Biol.* **2002**, *6*, 243−249.

(39) Zampella, G.; Bruschi, M.; Fantucci, P.; Razavett, M.; Pickett, C. J.; De Gioia, L. Dissecting the Intimate Mechanism of Cyanation of {2Fe3S} Complexes Related to the Active Site of All-Iron Hydrogenases by DFT Analysis of Energetics, Transition States, Intermediates and Products in the Carbonyl Substitution Pathway. *Chem.−Eur. J.* **2005**, *11*, 509−520.

(40) Bruschi, M.; Fantucci, P.; De Gioia, L. Density Functional Theory Investigation of the Active Site of Fe-Hydrogenases. Systematic Study of the Effects of Redox State and Ligands Hardness on Structural and Electronic Properties of Complexes Related to the [2Fe](H) Subcluster. *Inorg. Chem.* **2004**, *43*, 3733−3741.

(41) Eilers, G.; Schwartz, L.; Stein, M.; Zampella, G.; de Gioia, L.; Ott, S.; Lomoth, R. Ligand Vs. Metal Protonation of An Iron Hydrogenase Active Site Mimic. *Chem.−Eur. J.* **2007**, *13*, 7075−7084.

(42) Koningsberger, D. C.; Mojet, B. I.; Van Dorssen, G. E.; Ramaker, D. E. XAFS Spectroscopy; Fundamental Principles and Data Analysis. *Top. Catal.* **2000**, *10*, 143−155.

(43) Scott, R. A. X-ray Absorption Spectroscopy. In *Physical Methods in Bioinorganic Chemistry*; Que, L., Jr., Ed.; University Science Books: Sausalito CA, 2000; pp 465−503.

(44) Dau, H.; Liebisch, P.; Haumann, M. X-ray Absorption Spectroscopy to Analyze Nuclear Geometry and Electronic Structure of Biological Metal Centers-Potential and Questions Examined with Special Focus on the Tetra-Nuclear Manganese Complex of Oxygenic Photosynthesis. *Anal. Bioanal. Chem.* **2003**, *376*, 562−583.

Materials and Methods

Complex **1** = $[Fe_2(\mu\text{-}SCH_2N(CH_2Ph)CH_2S)(CO)_4(PMe_3)_2]$ was synthesized as described previously.[32] Its unprotonated form **1′** in solution and the protonated forms **[1H]**$^+$ = $[Fe_2(\mu\text{-}SCH_2NH(CH_2Ph)CH_2S)(CO)_4(PMe_3)_2]^+$, **[1HHy]**$^{2+}$ = $[Fe_2(\mu\text{-}H)(\mu\text{-}SCH_2NH(CH_2Ph)CH_2S)(CO)_4(PMe_3)_2]^{2+}$, and **[1Hy]**$^+$ = $[Fe_2(\mu\text{-}H)(\mu\text{-}SCH_2N(CH_2Ph)CH_2S)(CO)_4(PMe_3)_2]^+$ were prepared as outlined in ref 32. The freshly prepared samples at concentrations of the complexes of ∼10 mM (corresponding to ∼20 mM iron) in dried-acetonitrile solution were filled into specialized Kapton-covered gas-tight Delrin sample holders for XAS measurements under strict exclusion of dioxygen and immediately frozen in liquid nitrogen until use at the synchrotron radiation sources.

Infrared absorption spectra were recorded on a Bruker FTIR spectrometer (IFS 66v/S) as previously described[32] on the original samples in the holders later used for X-ray absorption spectroscopy (XAS) measurements.

XAS was performed at beamline D2 of the EMBL outstation (at HASYLAB, DESY: Hamburg, Germany) and at beamline KMC-1 of the BESSY (Berlin, Germany) on sample sets of all four complexes each. At beamline D2, EXAFS data up to k = 20 Å^{-1} (∼1530 eV above E_0) were measured; at BESSY the range was restricted to k = 18.5 Å^{-1} (∼1280 eV above E_0). K_α-fluorescence-detected XAS spectra at the iron K-edge were collected at 20 K using the energy-resolving germanium detectors (13-element at DESY, single-element at BESSY) and helium cryostat setups at the two beamlines as previously described.[45,46] Harmonic rejection was obtained by detuning the monochromators (Si(111) double crystal) to 50% of their peak intensity. XAS spectra collected at the two beamlines in a specific state were almost indistinguishable and averaged to yield a final data set of four spectra of the four protonation states. XAS spectra were corrected for detector dead-time, which was kept well below 25%, and averaged (6−10 scans) after energy calibration of each scan on the basis of a Gaussian fit to the peak at 7111.2 eV[47] present in the first derivative of the absorption spectrum of an iron foil (estimated accuracy in edge energy of better than ± 0.1 eV), which was measured simultaneously in absorption mode (not shown). Spectra were normalized, and EXAFS oscillations were extracted as described in ref 44. The energy scale of EXAFS spectra was converted to the wave-vector-scale (k-scale) using an E_0 value of 7112 eV. Unfiltered k^3-weighted spectra were used for least-squares curve-fitting and for calculation of Fourier-transforms (FTs). FTs were calculated from k-values ranging over 2−20 Å^{-1} (Figure 3) and over 3−18.5 Å^{-1} (Figure 4) and employing cos^2 window functions extending over 10% at both ends of the k-range. Multiple-scattering (MS) EXAFS simulations were performed on a PC using the program DL-EXCURV.[48]

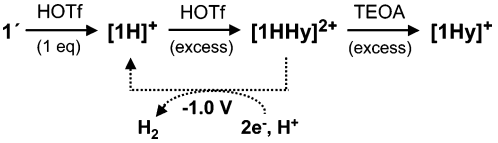

Figure 2. Sequence of protonation reactions of **1′** (**1** in acetonitrile solution) leading to its respective singly and doubly protonated derivatives, as established previously.[32,41] HOTf, triflic acid; TEOA, triethanolamine. As an example of one possible reaction path yielding H_2 evolution from the bridging hydride and a proton of the medium, the double reduction at the relatively positive potential of −1.0 V of **[1HHy]**$^{2+}$ to yield **[1H]**$^+$ is indicated.[32,41]

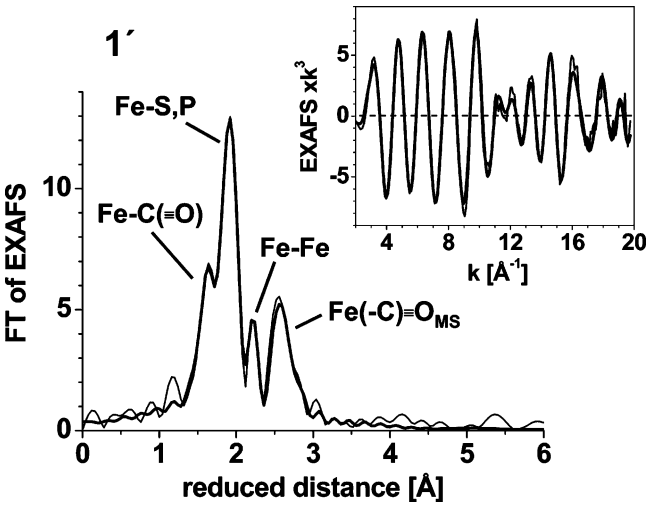

Figure 3. Fourier-transform (FT) of EXAFS oscillations (shown in the inset) of the unprotonated **1′** in acetonitrile solution at 20 K. The contributions of the individual iron-backscatterer interactions to the spectrum are indicated. Thin line, experimental data; thick line, simulation with the parameters given in Table 1. Prominent multiple-scattering (MS) contributions to the spectrum result from the linear Fe(−C)≡O bonding arrangement.

MS EXAFS fits were performed on the basis of a model, which was cut out from the crystal structure of **1** and included one absorbing iron atom and its two CO groups and one phosphorus and two sulfur ligands; the sulfur atoms were connected to the second iron atom. The default values of the DL-EXCURV program were utilized for MS calculations up to third-order scattering paths in the framework of curved-wave theory. An amplitude reduction factor S_0^2 = 0.9, which yielded the correct coordination numbers N_i with respect to the crystal structure of **1** if N_i values were allowed to vary in the simulations, was used in the EXAFS fits. The R-value (error) as calculated by the *DL_EXCURV* program was between 25 and 30% in the simulations. Alternatively, single-scattering joint-simulations of EXAFS spectra were performed with the in-house software *SimX*[49] and phase functions calculated by *FEFF-7*,[50] as previously described.[44]

Ab initio multiple-scattering XANES calculations were performed as described in ref 51 using the code *FEFF-8.2*[52] with the full-multiple-scattering and the self-consistent-field options activated (for further technical details, see ref 51). Atomic coordinates of FEFF input files for XANES calculations were generated using the iron-ligand distances derived from the EXAFS simulations and

(45) Buhrke, T.; Löscher, S.; Lenz, O.; Schlodder, E.; Zebger, I.; Andersen, L. K.; Hildebrandt, P.; Meyer-Klaucke, W.; Dau, H.; Friedrich, B.; Haumann, M. Reduction of Unusual Iron-Sulfur Clusters in the H_2-Sensing Regulatory Ni-Fe Hydrogenase from Ralstonia, Eutropha H16. *J. Biol. Chem.* **2005**, *280*, 19488−19495.

(46) Barra, M.; Haumann, M.; Loja, P.; Krivanek, R.; Grundmeier, A.; Dau, H. Intermediates in Assembly by Photoactivation After Heat-Induced Disassembly of the Manganese Complex of Photosynthetic Water Oxidation. *Biochemistry* **2006**, *45*, 14523−14532.

(47) Zhang, Y.; Pavlosky, M. A.; Brown, C. A.; Westre, T. E.; Hedman, B.; Hodgson, K. O.; Solomon, E. I. Spectroscopic and Theoretical Description of the Electronic Structure of the $S = {}^3/_2$ Nitrosyl Complex of Non-Heme Iron Enzymes. *J. Am. Chem. Soc.* **1992**, *114*, 9189−9191.

(48) Tomic, S.; Searle, B. G.; Wander, A.; Harrison, M. N.; Dent, A. J.; Mosselmans, J. F. W.; Inglesfield, J. E. *New Tools for the Analysis of EXAFS: The DL_EXCURV package*; CCLRC Technical Report DL-TR-2005−001, ISSN 1362−0207, 2005.

(49) Pospisil, P.; Haumann, M.; Dittmer, J.; Sole, V. A.; Dau, H. Stepwise Transition of the Tetra-Manganese Complex of Photosystem II to a Binuclear $Mn_2(\mu\text{-}O)_2$ Complex in Response to a Temperature Jump: A Time Resolved Structural Investigation Employing X-ray Absorption Spectroscopy. *Biophys. J.* **2003**, *84*, 1370−1386.

(50) Zabinsky, S. I.; Rehr, J. J.; Aukudinov, A.; Albers, R. C.; Eller, M. J. Multiple-Scattering Calculations of X-ray-Absorption Spectra. *Phys. Rev. B* **1995**, *52*, 2995−3009.

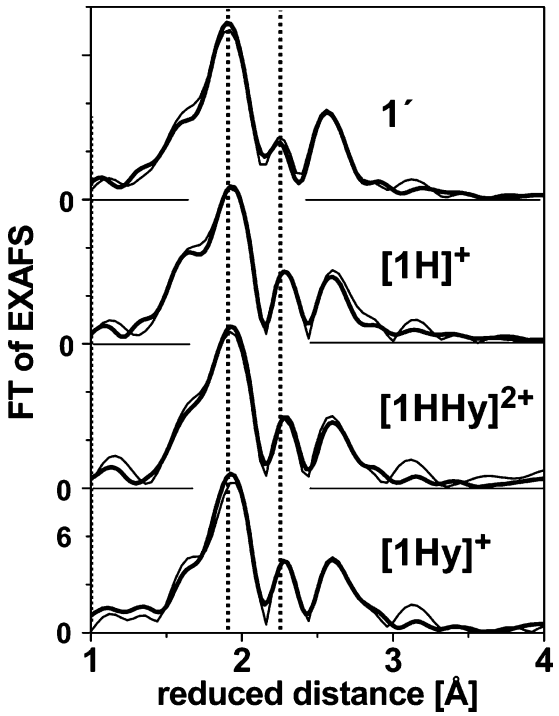

Figure 4. Fts of EXAFS oscillations of **1** in its four protonation states. Thin lines, experimental data; thick lines, simulation results including the parameters shown in Figure 5 (also Table 1).

employing the crystal structure of **1**[32] as a template. Calculated XANES spectra were shifted by 3 eV to lower energies for better comparison with the experimental spectra. No further attempts were made to improve the matching between experimental and calculated XANES spectra. For further details, see the Results section.

From XANES spectra, the pre-edge peak region was extracted by the subtraction of a polynomial spline through the main-edge rise using the program *Xanda*.[53][51] The line shape of the pre-edge peaks was readily reproduced by fitting the data using a least-squares algorithm to one or two Gaussian functions. (The inclusion of Lorentzians in the fit procedure was not required because the line width was largely determined by the energy resolution of the monochromators and not by lifetime broadening.) The K-edge energy was determined by the integral method, which has been shown to yield an almost linear relation between metal oxidation state and edge energy,[54] using integration limits of 15 and 90% of normalized fluorescence intensity (ref 44).

Density functional theory (DFT) calculations were carried out as follows. Cluster models of **1′**, **[1H]**$^+$, **[1Hy]**$^+$, and **[1HHy]**$^{2+}$ were geometry-optimized using the BP86[55,56] exchange-correlation functional and a TZVP basis set.[57] This functional has been shown before to yield structural parameters in excellent agreement with X-ray structures of hydrogenases.[84] The resolution-of-identity method was employed to accelerate the evaluation of Coulomb matrices.[58−61] A conductor-like screening model (COSMO) was used self-consistently to incorporate the solvent effects from acetonitrile ($\epsilon = 37$).[62−64] The minimum character of all of the structures was ensured by the absence of imaginary frequencies in numerically calculated second derivatives. All of the calculations were performed with the *ORCA* set of programs.[65] Atomic charges and bond-order analyses were done using the algorithms by Mayer.[66,67] Natural atomic orbital and natural bond-order analyses were performed using NBO5.0.[68]

Results

Preparation of the Four Complexes and Verification of the Yields by IR Spectroscopy. 1 (part B of Figure 1) was synthesized as reported in ref 32. Its dissolution in acetonitrile and freezing at 20 K yielded the unprotonated form here denoted as **1′**. Upon the addition of various acids (ref 32 for details), three differently protonated derivatives were formed[32,41] (Figure 2), namely **[1H]**$^+$ (protonation at the nitrogen atom of the adt moiety), **[1HHy]**$^{2+}$ (protonation both of the *N*-adt and of the Fe−Fe bond formally yielding a bridging hydride), and **[1Hy]**$^+$ (only the bridging hydride is present). The formation of the respective protonation states was verified by IR-spectroscopy (at room temperature,

(51) Burgdorf, T.; Löscher, S.; Liebisch, P.; van der Linden, E.; Galander, M.; Lendzian, F.; Meyer-Klaucke, W.; Albracht, S. P. W.; Friedrich, B.; Dau, H.; Haumann, M. Structural and Oxidation-State Changes at Its Nonstandard Ni−Fe Site During Activation of the NAD-Reducing Hydrogenase From *Ralstonia eutropha* Detected by X-ray Absorption, EPR, and FTIR Spectroscopy. *J. Am. Chem. Soc.* **2005**, *127*, 576−592.

(52) Ankudinov, A. L.; Ravel, B.; Rehr, J. J.; Conradson, S. D. Real-Space Multiple-Scattering Calculation and Interpretation of X-ray-Absorption Near-Edge Structure. *Phys. Rev. B* **1998**, *58*, 7565−7576.

(53) Klementiev, K. V. *XANES dactyloscope for Windows*; freeware: www.desy.de/∼klmn/xanda.html, 2005.

(54) Magnuson, A.; Liebisch, P.; Högblom, J.; Anderlund, M.; Lomoth, R.; Meyer-Klaucke, W.; Haumann, M.; Dau, H. Bridging-Type Changes Facilitate Successive Oxidation Steps at about 1 V in Two Binuclear Manganese Complexes − Implications for Photosynthetic Water Oxidation. *J. Inorg. Biochem.* **2006**, *100*, 1234−1243.

(55) Perdew, J. P. Density-Functional Approximation for the Correlation Energy of the Inhomogeneous Electron Gas. *Phys. Rev. B* **1986**, *33*, 8822−8824.

(56) Becke, A. D. Density-Functional Exchange-Energy Approximation with Correct Asymptotic Behavior. *Phys. Rev. A* **1988**, *38*, 3098−3100.

(57) Schäfer, A.; Horn, H.; Ahlrichs, R. Fully Optimized Contracted Gaussian Basis Sets for Atoms Li to Kr. *J. Chem. Phys.* **1992**, *97*, 2571−2577.

(58) Eichkorn, K.; Treutler, O.; Ohm, H.; Häsler, M.; Ahlrichs, R. Auxiliary Basis Sets to Approximate Coulomb Potentials. *Chem. Phys. Lett.* **1995**, *240*, 283−289.

(59) Eichkorn, K.; Treutler, O.; Ohm, H.; Häsler, M.; Ahlrichs, R. Auxiliary Basis Sets to Approximate Coulomb Potentials. *Chem. Phys. Lett.* **1995**, *242*, 652−660.

(60) Eichkorn, K.; Weigend, F.; Treutler, O.; Ahlrichs, R. Auxiliary Basis Sets for Main Row Atoms and Transition Metals and Their Use to Approximate Coulomb Potentials. *Theor. Chem. Acc.* **1997**, *97*, 119−124.

(61) Neese, F. An Improvement of the Resolution of the Identity Approximation for the Formation of the Coulomb Matrix. *J. Comput. Chem.* **2003**, *24*, 1740−1747.

(62) Andzelm, J.; Kölmel, C.; Klamt, A. Incorporation of Solvent Effects into Density Functional Calculations of Molecular Energies and Geometries. *J. Chem. Phys.* **1995**, *103*, 9312−9320.

(63) Klamt, A.; Schüürmann, G. COSMO: A New Approach to Dielectric Screening in Solvents with Explicit Expressions for the Screening Energy and Its Gradient. *J. Chem. Soc., Perkin Trans.* **1993**, *2*, 799−805.

(64) Sinnecker, S.; Rajendran, A.; Klamt, A.; Diedenhofen, M.; Neese, F. Calculation of Solvent Shifts on Electronic g-Tensors with the Conductor-Like Screening Model (COSMO) and Its Self-Consistent Generalization to Real Solvents (direct COSMO-RS). *J. Phys. Chem. A* **2006**, *110*, 2235−2245.

(65) Neese, F. Definition of Corresponding Orbitals and the Diradical Character in Broken Symmetry DFT Calculations on Spin Coupled Systems. *J. Phys. Chem. Solids* **2004**, *65*, 781−785.

(66) Mayer, I. Charge, Bond Order and Valence in the Ab Initio SCF Theory. *Chem. Phys. Lett.* **1983**, *97*, 270−274.

(67) Mayer, I. Bond Order and Valence: Relations to Mulliken's Population Analysis. *Int. J. Quantum Chem.* **1984**, *26*, 151−154.

(68) Glendening, E. D.; Badenhoop, J. K.; Reed, A. E.; Carpenter, J. E.; Bohmann, J. A.; Morales, C. M.; Weinhold, F. Theoretical Chemistry Institute: University of Wisconsin, Madison WI, U.S.A., 2001.

Table 1. Simulation Parameters of the EXAFS Spectrum of **1′** in CH_3CN Solution[a]

vector	N_i [per Fe]	R_i [Å]	$2\sigma^2_i$ [Å^2]
Fe−C(≡O)	2	1.756(5) [1.758]	0.003
Fe−S/P	3	2.226(5) [2.243]	0.004
Fe−Fe	1	2.526(5) [2.546]	0.002
Fe(−C)≡O_{MS}	2	2.948(10) [2.919]	0.004

[a] Iron−ligand distances as found in the crystal structure[32] are given in brackets.

Supporting Information and refs 32 and 41). Quantification of the respective IR band intensities (not documented) indicated that the purity of the four protonation states of **1** in solution was >90%.

EXAFS Analysis Reveals Significant Structural Differences in the Four Protonation States. EXAFS spectra were measured on two sets of samples of **1** in its four protonation states. The Fourier-transform (FT) of the EXAFS oscillations ranging up to $k = 20$ Å^{-1} of **1′** (unprotonated form) in frozen acetonitrile solution shows four major peaks (Figure 3, thin line) at reduced distances <3 Å (corresponding to the true iron-ligand distances minus ∼0.4 Å due to a phase shift), immediately revealing the presence of four dominant iron-backscatterer vectors as expected, according to the crystal structure of **1**.[32] The first three peaks are attributable to Fe−C(≡O), Fe−S, P, and Fe−Fe interactions, respectively. (Sulfur and phosphorus cannot easily be distinguished in EXAFS spectroscopy because of their comparable backscattering amplitude.) Peak four results from Fe(−C)≡O interactions, which are enhanced by multiple-scattering (MS) contributions due to the near-linear Fe−C≡O bonding arrangement. A convincing simulation (Figure 3, thick lines) of the EXAFS spectrum of **1′** was obtained with the best-fit parameters listed in Table 1. We used a multiple-scattering curved-wave algorithm to optimize a simplified model derived on the basis of the crystal structure, which was employed as a starting point (Materials and Methods). The mean iron-backscatterer distances of **1′** (Table 1), on average, appeared to be slightly shorter than those in the room-temperature crystal structure of **1**.[32] In part, the shortening may be due to the much lower temperature (20 K) in the EXAFS experiments (but see below). Any indications for contaminations of the samples, for example, by degradation products, were absent, in agreement with the IR results. The determined Fe−Fe distance of ∼2.53 Å in **1′** is similar to the Fe−Fe distances in related diiron compounds containing a μ-SRS motif (see, e.g., refs 34 and 86 for a compilation of respective crystallographically determined Fe−Fe distances). The analysis of the EXAFS spectrum clearly shows that the iron atoms in **1′** in solution possess the same ligands that are visible in the crystal structure of **1**. The alterations of the iron-ligand bond lengths in solution compared to the crystallized state are addressed in the following.

In Figure 4, the FTs of the EXAFS oscillations of the four protonation states are compared. Overall, the four spectra are relatively similar, revealing the absence of drastic structural changes of the complex upon protonation. (Indications for decomposition products also were absent.) However,

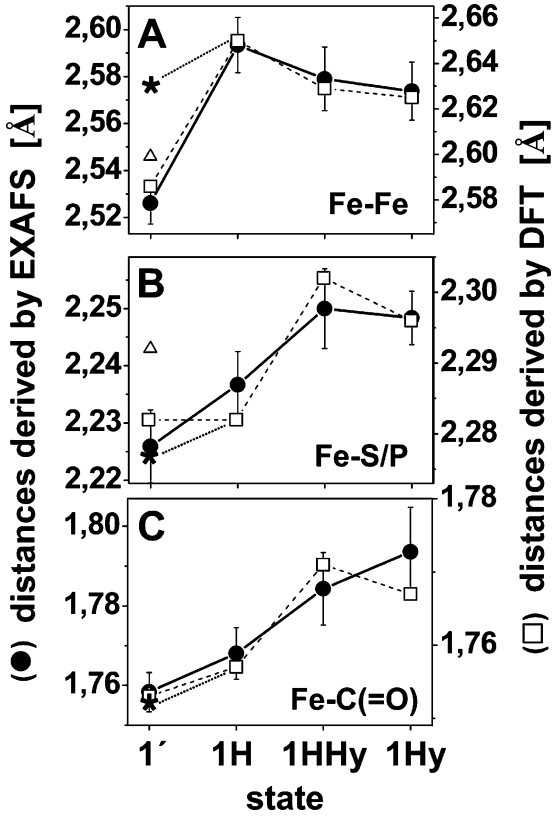

Figure 5. Selected iron-ligand distances in the four protonation states of **1**, as revealed by the EXAFS analysis (solid circles, left *y* axis) and by the DFT calculations (open squares, right *y* axis). EXAFS data represent the average of simulation results of two sets of spectra, using a multiple-scattering algorithm; the bars denote the respective absolute deviations from the mean values of parameters that were derived from simulations, where each spectrum was simulated separately or where the four spectra of each data set were simulated in a joint-fit approach.[49] DFT parameters are for calculations including the acetonitrile solvent. The distances in **1′** from DFT refer to the $\mathbf{1'_a}$ (open squares) and to the $\mathbf{1'_b}$ (asterisks) conformations, respectively (Figure 6). Open triangles represent the iron-ligand distances in the crystal structure of **1**.[32] Fe−C and Fe−S/P distances from DFT represent the average over the several respective iron-ligand interactions in the complex.

specific changes are discernible already by visual inspection of the FTs, namely a shift to higher distances of the FT peak due to Fe−S,P vectors at a reduced distance of ∼1.9 Å and of the peak due to the Fe−Fe vector at ∼2.3 Å (Figure 4, dotted lines), in the spectra of the protonated forms. The underlying structural changes were determined by EXAFS simulations (curve fitting).

The best-fit results (Figure 4, thick lines) revealed an interesting outcome (Figure 5). Already, upon protonation of **1′** at the nitrogen atom of its adt ligand (yielding $\mathbf{[1H]^+}$), the most pronounced structural change occurs. The Fe−Fe distance becomes elongated by ∼0.06 Å (Figure 5). Upon protonation of the Fe−Fe bond to yield a bridging hydride in $\mathbf{[1HHy]^{2+}}$ and $\mathbf{[1Hy]^+}$, the Fe−Fe distance is only slightly shortened compared to $\mathbf{[1H]^+}$. These results consistently were reproduced in a joint-fit approach[49] applied to the four spectra of two independent data sets (not documented). Further structural changes were resolved. The mean Fe−S,P distance is lengthened in $\mathbf{[1H]^+}$ compared to that in **1′**, but similar in $\mathbf{[1HHy]^{2+}}$ and $\mathbf{[1Hy]^+}$; there is an increase in the Fe−C(≡O) bond lengths predominantly upon the change from $\mathbf{[1H]^+}$

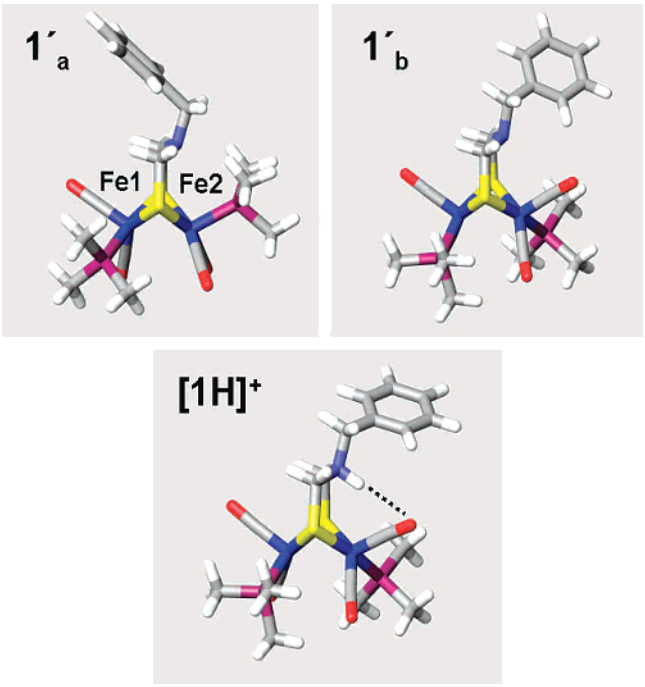

Figure 6. DFT structures of two rotamers of **1′** and of **[1H]**$^+$ protonated at the *N*-adt in acetonitrile. The conformation of **1** in the crystal structure[32] is similar to $\mathbf{1'_a}$; however, the benzol ring is rotated with respect to the adt moiety as shown for $\mathbf{1'_b}$. In **[1H]**$^+$, the complex is locked in a conformation that resembles $\mathbf{1'_b}$ with respect to the basal positioning of both PMe_3 groups; however, the benzol ring likely is oriented similar to that in in $\mathbf{1'_a}$.[32,41] The putative engagement of the proton on the *N*-adt in a hydrogen-bond with the apical carbonyl in **[1H]**$^+$ is indicated by the dotted line. Color code: Blue, iron; red, oxygen; light blue, nitrogen; magenta, phosphorus; yellow, sulfur; gray, carbon; white, hydrogen.

to **[1HHy]**$^{2+}$ where the hydride becomes bound (Figure 5). A slight increase of the iron-ligand distances is expected upon the binding of a sixth ligand to the iron atoms. In summary, the EXAFS analysis suggests that a significant structural change of **1′** is induced already upon protonation of its adt nitrogen, which is relatively remote from the two iron atoms (at distances of about 3.4 and 3.8 Å, respectively).

Calculation of Structures Using DFT and Comparison to Experimental Results. Geometry-optimized structures of **1** in its four protonation states in acetonitrile were calculated using density functional theory (DFT).[41] In Figure 5, the experimentally derived Fe−Fe distances are compared with those calculated by DFT. In the crystal structure of **1**, an Fe−Fe bond distance of 2.55 Å is observed. EXAFS analysis revealed an Fe−Fe distance of 2.53 Å in **1′** in acetonitrile solution. By DFT, the structures of two rotational isomers in acetonitrile ($\mathbf{1'_a}$ and $\mathbf{1'_b}$) were predicted (Figure 6), where either ($\mathbf{1'_a}$) the two PMe_3 ligands occupy apical-basal positions and the CO ligands are in eclipsed conformation as in the solid state or ($\mathbf{1'_b}$) the PMe_3 groups are trans-dibasal and the CO ligands are in staggered conformation. The calculated Fe−Fe distance for $\mathbf{1'_a}$ is 2.586 Å and very similar to that found in the crystal structure of **1**,[32] but for $\mathbf{1'_b}$, this distance is longer by 0.06 Å, namely 2.634 Å. Structural parameters from the X-ray analysis are reproduced by the DFT calculations within 0.03−0.04 Å for bond lengths and 1−2° for bond angles. Similar accuracy also has been achieved for models of the active site of hydrogenases using the same functional.[84] The transition from $\mathbf{1'_a}$ to $\mathbf{1'_b}$, involving the rotation of the PMe_3 group and of one CO around the Fe2 (Figure 6), was found to be slightly endergonic (ΔG = ~6.7 kJ mol^{-1}) when solvent effects are considered in the DFT calculations.

Previous ^{1}H and ^{31}P NMR results[32,41] suggested that, at room temperature, a species similar to $\mathbf{1'_b}$ is dominant in acetonitrile solution and present to ≥90%. Comparison of the Fe−Fe distance from EXAFS (2.53 Å) to those from crystallography (2.55 Å) and DFT (2.586 Å) suggests that, at the temperature of the EXAFS measurements (20 K), the prevailing form is similar to $\mathbf{1'_a}$ (Figures 5 and 6). Clearly, the calculated Fe−Fe distance of 2.63 Å in $\mathbf{1'_b}$ is significantly longer that that of $\mathbf{1'_a}$ (the distance difference is larger than the error of the calculated structural parameters). Accordingly, upon freezing of the samples to cryogenic temperatures, the slightly endergonic character of the $\mathbf{1'_a} \rightarrow \mathbf{1'_b}$ transition leads to an almost-complete bias at low temperatures toward a conformation similar to $\mathbf{1'_a}$, where the PMe_3 groups are in mixed basal/apical conformations.

In the DFT calculations, the Fe−Fe bond length increases by 0.02 Å for the $\mathbf{1'_b} \rightarrow$ **[1H]**$^+$ transition, but by 0.06 Å for the $\mathbf{1'_a} \rightarrow$ **[1H]**$^+$ transition, to 2.65 Å (Figure 5). An increase by ~0.06 Å was observed in the EXAFS data, corroborating the above notion that a species similar to $\mathbf{1'_a}$ is dominant at 20 K. In **[1H]**$^+$, apparently the complex is locked in a conformation that resembles that of $\mathbf{1'_b}$ and where the PMe_3 groups both occupy basal positions, at room temperature as well as at 20 K. The proton on the *N*-adt may be engaged in a hydrogen bond with the now apically coordinated CO ligand on Fe2, thereby stabilizing this conformation (Figure 6). In addition, there is a repositioning in **[1H]**$^+$ of the two CO ligands, which are below the Fe−Fe vector in $\mathbf{1'_a}$ (Figure 6) so that the Fe−Fe bond becomes more exposed to the solvent. When the hydride occupies the Fe−Fe bridging position in **[1HHy]**$^{2+}$ and **[1Hy]**$^+$, the slight decreases in the Fe−Fe distance from DFT are similar to those observed by EXAFS (Figure 5). Thus, the chosen level of theory in the DFT calculations was adequate to reproduce the structural changes observed in the XAS experiments. Notably, upon protonation of the Fe−Fe bond, in the related diiron compound (μ-edt)[Fe(CO)$_2$(PMe$_3$)]$_2$ (edt = SCH_2CH_2S), a lengthening of the Fe−Fe distance by ~0.06 Å and rotation of one PMe_3 group from the apical to basal position has been observed, whereas an increase in the Fe−Fe distance by only ~0.02 Å was determined for (μ-pdt)[Fe(CO)$_2$(PMe$_3$)]$_2$ (pdt = $SCH_2CH_2CH_2S$), which does not involve PMe_3 rotation.[34] These changes in the Fe−Fe distance are similar to those observed here for the $\mathbf{1'_a} \rightarrow$ **[1H]**$^+$ and $\mathbf{1'_b} \rightarrow$ **[1H]**$^+$ transitions, respectively.

In summary, comparison of the EXAFS- and DFT-derived distances of the Fe−Fe, Fe−S/P, and Fe−CO interactions and of the distance changes revealed a striking agreement between the two data sets (Figure 5). By both methods, even subtle changes in the structure of the complex upon protonation were resolved. In solution at ambient temperatures, the PMe_3 and CO ligands of the Fe atoms are free to rotate, yielding nearly isoenergetic complexes $\mathbf{1'_a}$ and $\mathbf{1'_b}$. At

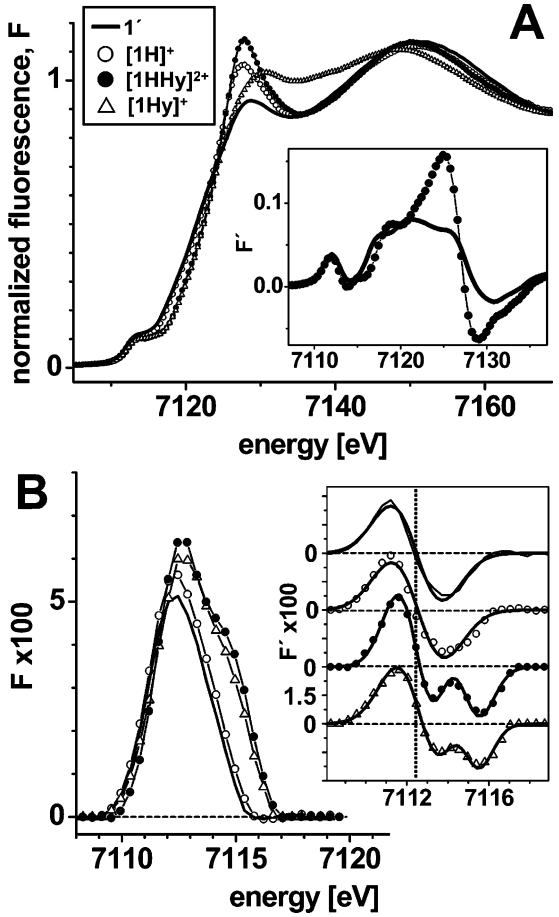

Figure 7. (A) XANES spectra of the four protonation states of **1**. Note the upshift in edge energy in complexes **[1HHy]**$^{2+}$ and **[1Hy]**$^{+}$. Inset: First derivatives of the spectra of **1** and **[1HHy]**$^{2+}$. (B) Preedge peak features extracted from the XANES spectra in (A). Inset: The respective first derivatives and simulation results (thick lines) on the basis of parameters shown in Table 2.

cryogenic temperature, $\mathbf{1'_a}$ is prevailing. The protonation of the *N*-adt locks the complex in a conformation similar to $\mathbf{1'_b}$, where the two PMe_3 groups are in basal positions and an elongation of the Fe−Fe bond and rotation of CO ligands has occurred. These changes may facilitate the protonation of the Fe−Fe bond to yield the bridging hydride. Because our studies show that the elongation of the Fe−Fe bond in **[1H]**$^{+}$ is caused by the adt protonation, this feature could be used to determine unambiguously whether an adt moiety or an all-carbon-based propyldithiolate is present in the iron-only H_2ases.

XANES Analysis to Track Hydride Binding to Fe. The XANES region of XAS spectra is particularly sensitive to changes in the first coordination sphere of metals.[44,69,70] XANES spectra of the four states of the complex are shown in part A of Figure 7. In general, the edge spectra of compounds with mixed S/P and C═O/N ligation of iron rarely have been reported. The overall edge shape of **1′** resembles that of the five-coordinated iron found in two enzymes. The single iron ion in CN-treated iron-sulfur-cluster-free hydrogenase (Hmd) from *Methanothermobacter marburgensis* is coordinated by two CO, one CN, one O/N, and one sulfur ligand.[71] The iron in the isolated large subunit of the regulatory Ni−Fe hydrogenase (RH) from *Ralstonia eutropha*, which is a H_2-sensor, is coordinated by two CN, one CO, and two sulfur ligands.[72] The main-edge energy of 7121.0 eV (Table 2) of **1′** is estimated to be by ∼1 eV lower compared to those of the above enzymes.[71,72] This energy value is sensitive both to the iron oxidation state and to the chemical nature and geometry of its ligands.[44] The energy of the pre-edge peak (below) may reflect the true metal oxidation state more precisely. It is 7112.5 eV in **1′** and by about 0.3 eV lower than that of RH and Hmd. In the RH, the presence of iron(II) is established;[72−74] in Hmd it may be realized.[75] For iron(I), the pre-edge peak energy may be expected to be ∼1 eV lower than that of iron(II).[76] The XANES results suggest that the two Fe atoms in **1′** on the average are slightly more electron rich (more reduced) than the iron(II) atom in RH (and Hmd), but less electron rich than expected, considering the formal iron(I)−iron(I) oxidation state of **1′**.[32]

Table 2. Parameters That Describe the Preedge Region of XANES Spectra

sample	E_{edge} [eV][a]	$E_{1s\rightarrow 3d}$/fwhm[eV][b]	$I_{1s\rightarrow 3d}$ [10^{-2} eV][c]
1′	7121.0	7112.5/2.5	15.9
[1H]$^{+}$	7121.1	7112.5/2.6	18.1
[1HHy]$^{2+}$	7121.6	7112.7/2.1	15.7
		7114.9/1.8	7.8
[1Hy]$^{+}$	7121.8	7112.7/2.3	18.2
		7115.0/1.6	4.2

[a] The edge energy has been obtained by the integral method.[44] [b] Energy and fwhm of pre-edge transitions as derived from simulations of the spectra. [c] Intensities of the transitions obtained by the integration of simulation curves.

The pronounced changes in the shape of the XANES spectra of the protonated forms of **1′** point to changes in the first-sphere ligand geometry around the iron atoms, in line with the bond length changes detected by the EXAFS analysis. Already, upon the protonation of **1′** at *N*-adt to yield

(69) Mijovilovitch, A.; Meyer-Klaucke, W. Simulating the XANES of Metalloenzymes − A Case Study. *J. Synchrotron Radiat.* **2003**, *10*, 64−68.

(70) Benfatto, S.; Della Longa, S.; Natoli, C. R. The MXAN Procedure: A New Method for Analysing the XANES Spectra of Metalloproteins to Obtain Structural Quantitative Information. *J. Synchrotron Radiat.* **2003**, *10*, 51−57.

(71) Korbas, M.; Vogt, S.; Meyer-Klaucke, W.; Bill, E.; Lyon, E. J.; Thauer, R. K.; Shima, S. The Iron-Sulfur-Cluster-Free Hydrogenase (Hmd) is a Metalloenzymes with a Novel Iron Binding Motif. *J. Biol. Chem.* **2006**, *281*, 30804−30813.

(72) Löscher, S.; Zebger, I.; Andersen, L. K.; Hildebrandt, P.; Meyer-Klaucke, W.; Haumann, M. The Structure of the Ni−Fe Site in the Isolated HoxC Subunit of the Hydrogen-Sensing Hydrogenase from *Ralstonia eutropha*. *FEBS lett.* **2005**, *579*, 4287−4291.

(73) Bernhard, M.; Buhrke, T.; Bleijlevens, B.; De Lacey, A. L.; Fernandez, V. M.; Albracht, S. P.; Friedrich, B. The H_2 Sensor of *Ralstonia eutropha*. *J. Biol. Chem.* **2001**, *276*, 15592−15597.

(74) Haumann, M.; Porthun, A.; Buhrke, T.; Liebisch, P.; Meyer-Klaucke, W.; Friedrich, B.; Dau, H. Hydrogen-Induced Structural Changes at the Nickel Site of the Regulatory [NiFe] Hydrogenase from *Ralstonia eutropha* Studied by X-ray Absorption Spectroscopy. *Biochemistry* **2003**, *42*, 11004−11015.

(75) Shima, S.; Lyon, E. J.; Thauer, R. K.; Mienert, B.; Bill, E. Mössbauer Studies of the Iron-Sulfur Cluster-Free Hydrogenase: The Electronic State of the Mononuclear Fe Active Site. *J. Am. Chem. Soc.* **2005**, *127*, 10430−10435.

(76) Westre, T. E.; Kennepohl, P.; DeWitt, J. G.; Hedman, B.; Hodgson, K. O.; Solomon, E. I. A Multiplet Analysis of the Fe K-Edge 1s → 3d Pre-Edge Features of Iron Complexes. *J. Am. Chem. Soc.* **1997**, *119*, 6297−6314.

[1H]$^+$, there is a pronounced increase of the primary maximum at ~7127 eV of the XANES spectrum. This increase suggests a more-homogeneous ligand environment of the two iron atoms in **[1H]**$^+$, in agreement with the EXAFS and DFT results. The edge energy, however, remains almost constant (Table 2), suggesting a similar mean iron oxidation state in **1′** and **[1H]**$^+$. The edge maximum and slope (part A of Figure 7, inset) is even larger in **[1HHy]**$^{2+}$, and, in addition, there is an increase of the edge energy by about 0.5 eV (Table 2). The edge energies of **[1HHy]**$^{2+}$ and **[1Hy]**$^+$ are similar. However, the overall edge shape of **[1Hy]**$^+$ differs from that of **[1HHy]**$^{2+}$, pointing to a more-heterogeneous ligand environment at the iron atoms in **[1Hy]**$^+$ due to the increased rotational freedom of the CO and PMe_3 ligands, in the absence of the proton at the adt.

The edge upshift of ~0.5 eV on the **1′**/**[1H]**$^+$ → **[1HHy]**$^{2+}$/**[1Hy]**$^+$ transition is too small to account for a single-electron iron oxidation, as already for the one-step oxidation of one out of the two iron atoms, an edge upshift by ≥1 eV may be expected.[74,76,77] The small edge upshift does not support the formally assumed oxidation of iron(I) in **1′** and **[1H]**$^+$ to iron(II) in **[1HHy]**$^{2+}$ and **[1Hy]**$^+$.[32] However, there is a pronounced shift of the CO stretching vibrations to higher frequencies on the **[1H]**$^+$ → **[1HHy]**$^+$ transition in the IR spectra,[32] indicating a substantial decrease in the negative charge density at the iron atoms upon Fe−Fe bond protonation. A likely interpretation of the XANES and IR results is that the iron oxidation state is in between iron(I) and iron(II) in **[1H]**$^+$ and that the equilibrium described by the resonance formula Fe(I)−H$^+$−Fe(I) ↔ Fe(II)−H$^-$−Fe(II) is only marginally biased toward the iron(II)$_2$ state in **[1HHy]**$^{2+}$. In line with this proposal, natural bond order (NBO) calculations revealed only slight changes of the negative charge density on the iron atoms and a slight increase in the positive charge on the sulfur ligands (changes by less than ± 0.1*e*) on the **[1H]**$^+$ → **[1HHy]**$^+$ transition. Accordingly, Fe−Fe bond protonation may be accompanied by partial iron and sulfur ligand-centered oxidations.

Remarkably, hydride binding clearly affects the pre-edge peak feature of the XANES spectrum, which is attributable to formally dipole-forbidden 1s → 3d electronic transitions (part B of Figure 7). The relatively large absolute pre-edge intensities (Table 2) in the spectra of **1** and **[1H]**$^+$ are typical for five-coordinated iron atoms[76] for which the 1s → 3d dipolar strength is enhanced relative to octahedral complexes due to 4p$_z$ orbital mixing into the electron final states. That only one dominant pre-edge peak was resolved in **1′** reflects the presence of a weak axial ligand field distortion where 1s → 3d$_{z^2}$ (+4*p*$_z$) is the strongest transition at the lowest energy.[76] The increased intensity of the pre-edge peak in **[1H]**$^+$ is in agreement with a redistribution of electric dipole intensity to lower energies; from the equatorial plane (3d$_{x^2-y^2}$ orbital) of trigonal-bipyramidal iron in **1′** to the axial direction (3d$_{z^2}$ (+4p$_z$) orbital) of square-pyramidal iron in **[1H]**$^+$. These geometrical attributions are corroborated by the XANES simulations descibed below.

Interestingly, in the spectra of **[1HHy]**$^{2+}$ and **[1Hy]**$^+$, a splitting of the pre-edge peak occurs (part B of Figure 7, inset). The shift of the low-energy pre-edge maximum by ~0.3 eV to higher energies may reflect the stabilization, at 20 K, of the electron final state due to decreased charge density at the iron atoms in the presence of the hydride. A second peak feature appears at ~7116 eV. The presence of the hydride causes a strong distortion of the ligand field of the previously square-pyramidal iron atoms (in **[1H]**$^+$) along the axial direction due to the additional short Fe−H bonds. Accordingly, the 3d$_{z^2}$ orbital increases in energy, decreasing its occupancy. Indeed, NBO calculations revealed a decreased occupancy (by ~0.06*e*) of the 3d$_{z^2}$ orbitals (average over both iron atoms) in **[1HHy]**$^{2+}$ compared to that for **[1H]**$^+$. This effect and additional 4p$_z$ mixing into the 3d$_{z^2}$ and 3d$_{x^2-y^2}$ orbitals enhance the intensities of the respective electronic transitions.[76,78] Noteworthy, altered intensity of low-lying electronic transitions also has been detected in nickel XANES spectra of Ni−Fe hydrogenases upon the binding of hydrogen species to the nickel[51,79] and in metallic hydrides.[80] In conclusion, the presence of the hydride is revealed in the XANES spectra of **[1HHy]**$^{2+}$ and **[1Hy]**$^+$. XANES changes thus may serve as a diagnostic feature for metal-hydride interactions in model compounds and enzymes.

Ab initio XANES calculations[44,51,52] were performed to derive further information on changes in the ligand geometry around the iron atoms in the four protonation states of the complex. A XANES spectrum that was calculated using the crystallographic coordinates of **1**[32] was unlike the experimental spectrum of **1′** because the primary edge maximum at ~7128 eV was considerably larger (bottom of part B of Figure 8, dashed line). Already, calculations on a relatively simple model (part A-a of Figure 8), which comprised only one iron atom and its primary ligands (2x CO, 1x PMe_3, 2x SH_2), and the respective iron-ligand distances derived by the EXAFS analysis readily reproduced the main features, in particular the small primary edge maximum of the XANES spectrum of **1′** (bottom of part B of Figure 8, solid line). This model comprises a near trigonal-bipyramidal geometry of the ligands (part A-a of Figure 8), where the two CO groups and one sulfur atom are about in the same plane, and the phosphorus atom and the second sulfur point to the respective directions perpendicular to this plane. Exchange of the positions of the phosphorus ligand and the axial CO ligand, under retention of the overall geometry, yielded a

(77) Petit, P. E.; Farges, F.; Wilke, M.; Sole, V. A. Determination of the Iron Oxidation State in Earth Materials Using XANES Pre-Edge Information. *J. Synchrotron Radiat.* **2001**, *8*, 292−294.

(78) Westre, T. E.; Loeb, K. E.; Zaleski, J. M.; Hedman, B.; Hodgson, K. O.; Solomon, E. I. Determination of the Geometric and Electronic Structure of Activated Bleomycin Using X-ray Absorption Spectroscopy. *J. Am. Chem. Soc.* **1995**, *117*, 1309−1313.

(79) Löscher, S.; Burgdorf, T.; Zebger, I.; Hildebrandt, P.; Dau, H.; Friedrich, B.; Haumann, M. Bias from H_2-Cleavage to -Production and Coordination Changes at the Ni−Fe Site in NAD^+-Reducing Hydrogenase from *Ralstonia eutropha*. *Biochemistry* **2006**, *45*, 11658−11665.

(80) Kochubei, D. I.; Kriventsov, V. V.; Maksimov, Y. V.; Tsodikov, M. V.; Vandieva, F. A.; Mordvin, V. P.; Navio, J. A.; Moiseev, II. Intermetallic Hydrides $[TiFe_{0.95}Zr_{0.03}Mo_{0.02}]H_x$ ($0 \leq \times \leq 2$): The Nature of the Phase Responsible for the Selective Reduction of CO_2. *Kinet. Catal.* **2003**, *44*, 163−174.

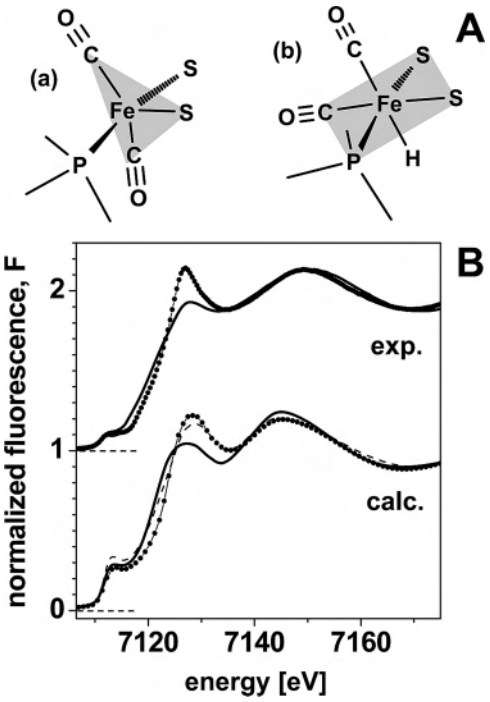

Figure 8. (A) Approximate model structures underlying the ab initio calculations of the XANES spectra shown in (B). The shaded areas encompass atoms lying in about the same plane. (B) Experimental XANES spectra (top; **1**, line and **[1HHy]**$^{2+}$, dots) and respective calculated spectra (bottom; the dashed line represents a spectrum calculated on the basis of the crystal coordinates of **1**). For further details, see the body of the text.

similar spectrum (not shown), which showed an only slightly increased primary maximum. These results suggest that the differences in the XANES spectra of **1′** (in a conformation at 20 K similar to **1′**$_{\mathbf{a}}$) and **[1H]**$^{+}$ (in a **1′**$_{\mathbf{b}}$-like conformation) are not only attributable to the change from an apical to a basal position of the PMe_3 group on Fe2 but also to changes in the overall ligand geometry. A satisfactory simulation (bottom of part B of Figure 8, circles), reproducing the larger primary maxima of the XANES spectra of **[1H]**$^{+}$ and **1HHy]**$^{+}$ only was obtained using a near square-pyramidal iron coordination (part A-b of Figure 8), no matter whether the phosphine group was in the basal or apical position. The presence or absence of the hydride had almost no effect on the spectral shape.

In conclusion, a near trigonal-bipyramidal iron coordination may be present in **1′** in frozen solution. In such a ligand geometry, the two CO groups below the Fe−Fe axis (compare Figure 6) may sterically hinder the binding of the hydride. Upon protonation of the *N*-adt in **[1H]**$^{+}$, near square-pyramidal coordinated iron atoms are formed, leading to an increase in the Fe−Fe distance accompanied by CO reorientation, thereby opening the binding site for the bridging hydride.

Electronic Calculations on the Four Complexes and Energetics of the Structural Changes. Relevant electronic features of the four protonation states were calculated to shed light on the energetics of the structural changes. Mayer bond-order analysis is a means to estimate the number of electrons shared between two metal atoms.[66,67] The theoretical bond order is unity in perfectly homodiatomic molecules but decreases for polar bonding situations and charge interactions and delocalization. In the calculated structures **1′**$_{\mathbf{a/b}}$ and in that of **[1H]**$^{+}$ comprising the protonated *N*-adt, the Fe−Fe bond order is similar (0.49/0.48 vs 0.48), although there is a significant increase in the Fe−Fe distance. **[1HHy]**$^{2+}$ and **[1Hy]**$^{+}$ exhibit a significantly lower Fe−Fe Mayer bond orders (0.315 and 0.305) than the complexes with a vacant bridging position, possibly reflecting an increase in charge delocalization in the complex in the presence of the additional Fe−μH−Fe bond. That the bond order in the DFT structure of **[1H]**$^{+}$ is not increased relative to **1′**$_{\mathbf{a/b}}$ suggests that an enhanced basicity of the Fe−Fe bond, which may be expected upon the *N*-adt protonation with the associated structural changes, does not govern the Fe−Fe bond protonation.

However, the Fe−Fe bond protonation is calculated to be thermodynamically favored by about 12 kJ mol^{-1} over *N*-adt protonation. This result raises the question why the Fe−Fe bond is not protonated first. The preformation energies, that are the total energies required to adopt the geometry of **1′**$_{\mathbf{a/b}}$ to the protonated forms, are calculated to be 31.3/28.3 kJ mol^{-1} for the **1′**$_{\mathbf{a/b}}$ → **[1Hy]**$^{+}$ transitions, but smaller, 28.1/25.4 kJ mol^{-1} for **1′**$_{\mathbf{a/b}}$ → **[1H]**$^{+}$. The lower energy requirement to form **[1H]**$^{+}$ may explain why the protonation at the *N*-adt occurs first (and is kinetically favored, as previously observed[41]) and not the hydride binding. In other words, a considerable amount of the energy demand, that is required to form a complex where hydride binding is feasible, already may be covered by the initial protonation of the adt nitrogen. Thus, the protonation of the adt nitrogen at least partially facilitates the subsequent hydride binding.

The XAS results suggest that a significant reorientation of CO ligands occurs upon *N*-adt protonation so that the Fe−Fe bond may become more accessible. In the oxidized state of iron-only hydrogenases, one CO is located in a semibridging position.[6] In **1′** at room-temperature, such a situation is not anticipated according to previous IR results.[32,41] By the calculation of the Gibbs free energy differences (ΔG), we investigated the energetics of the formation of a bridging CO in conformation **1′**$_{\mathbf{b}}$. In the respective calculated structure (not shown), the Fe−Fe distance decreases (by 0.02 Å) with respect to the situation where the CO is terminally coordinated; the Fe−C(=O) distances are 2.30 and 1.76 Å, respectively. The semibridging coordination of the CO ligand is disfavored by an energy amount of about 33 kJ mol^{-1}. Taking into account the large negative entropic contributions to the formation of a semibridging CO (and considering thermal corrections), this energy difference may increase (at 298 K) to yield a ΔG of ∼168 kJ mol^{-1}. In the calculated structure of **[1H]**$^{+}$, a semibridging CO is even more unfavorable (the respective Fe−C(=O) distances are 2.63 and 1.75 Å), the ΔG value for its formation (at 298 K) is ∼190 kJ mol^{-1}. Thus, by protonation of the *N*-adt, a CO in a bridging position where it disables hydride binding is calculated to become disfavored by ∼40 kJ mol^{-1}. Obviously, in the iron-only H_2ases, formation of a semibridging CO energetically is feasible as it is observed in the crystal structure.[6,9] It is tempting to speculate that the protonation of the putative adt nitrogen in the enzymes energetically

disfavors a bridging CO similar to the situation in **1**, thereby causing the movement of the bridging CO to a terminal position, as observed in the crystal structure of reduced iron-only H_2ase[7,9] and enabling hydride binding.

Discussion

Structural changes of an Fe−Fe hydrogenase active-site biomimetic compound, **1** ($[Fe_2(\mu\text{-}SCH_2N(CH_2Ph)CH_2S)(CO)_4(PMe_3)_2]$),[32,41] were investigated in four distinct protonation states using XAS at the iron K-edge. The structural parameters derived by DFT calculations are in excellent agreement with those determined by XAS. Accordingly, both methods provide complementary information to reliably assign structural features at the atomic level in biomimetic compounds, aiming at the elucidation of the mechanism of H_2 catalysis in hydrogenases.

Our main findings can be summarized as follows. (1) Both iron atoms in **1′** seem to adopt near trigonal-bipyramidal coordination geometries in CH_3CN solution, more pronounced at 20 K than at room temperature, so that the CO ligands sterically may hinder the access of a proton to the Fe−Fe bond. (2) The most prominent structural changes of the complex occur already upon the protonation of the adt nitrogen in $\mathbf{[1H]}^+$; the complex is locked in a conformation with both its phosphine groups occupying basal positions at the iron atoms. (In **1′**, in frozen solution, and in the crystal structure,[32] one phosphine group is in the apical position.) (3) A significant increase in the Fe−Fe distance and a near square-pyramidal iron coordination geometry in $\mathbf{[1H]}^+$ render the Fe−Fe bond more accessible to protonation. In turn, the lengthening of the Fe−Fe bond upon protonation at the *N*-adt could be used as a probe to verify the nature of the dithiolate tether in the iron-only hydrogenases. (4) The binding of the formal hydride in the Fe−Fe bridging position in $\mathbf{[1HHy]}^{2+}$ and $\mathbf{[1Hy]}^+$ is revealed by a splitting of the pre-edge peak in the XANES spectra. Hydride binding only marginally affects the overall structure of the complex. The presence of a bridging hydride in $\mathbf{[1HHy]}^{2+}$ and $\mathbf{[1Hy]}^+$ previously has been inferred from ^{1}H NMR data[32,41] and is supported by the XAS results and DFT calculations in the present work.

The detected structural changes and the computational results in this work suggest the facilitated formation of a hydride binding site in **1** upon *N*-adt protonation. A general feature of $(\mu\text{-}SRS)[Fe(X)_3]_2$ compounds (R is an organic linker, X is CO, CN, or PMe_3) is the ease with which molecular rearrangements occur (refs 28, 30, and references therein). In solutions of **1**, stereochemical nonrigidity with respect both to the rotation of CO and PMe_3 groups and to symmetry inversion of the benzylic moiety of the adt is observed.[32] On the one hand, such a flexibility disfavors apical positions (of the phosphines in **1**) at least at room temperature. On the other hand, CO ligands may be oriented in a way that they sterically hinder proton access to the Fe−Fe bond.[12] Notably, in an $Fe_2(CO)_5$ compound, in solution, even a bridging CO has been detected in the reduction pathway.[81] In **1**, a bridging CO is not observed. In the presence of adt-NH^+ (in $\mathbf{[1H]}^+$ and $\mathbf{[1HHy]}^+$), symmetry inversion of the adt-phenyl is disabled (according to previous ^{31}P NMR data[32] and to the results in this work) and the PMe_3 groups are poised in basal positions so that the apical positions are occupied by CO. A possible explanation for the stabilization of this structure is the formation of a hydrogen bond between the NH^+ and an apical CO, as suggested by the DFT calculations. We note that previously calculated IR-band frequencies of the CO groups on the basis of DFT-optimized structural models and the experimental spectra are in good agreement.[41]

The structural changes on the transition from **1′** to $\mathbf{[1H]}^+$, according to our calculations, are energetically costly, in agreement with the unusual low basicity observed for the tertiary *N*-adt.[41] In related compounds, for the rotation of an axial CO ligand and similar lengthening of the Fe−Fe bond as observed in this study, the energy requirements are on the order of tens of kilojoules per mole.[18,39] We postulate that, by the protonation of the *N*-adt, a large amount of the energy, which is required to adopt the complex to a structure favoring subsequent hydride binding, already is covered. Indeed, in certain Ni−Fe hydrogenase models, the ligand reorganization has been found to be the most-unfavorable step along the H_2-cleavage reaction path.[82] One prerequisite for high-turnover H_2-formation catalysts thus may be the accessibility of protonation sites without major structural changes. Alternatively, the catalyst may be preactivated, for example, by protonation. In electrochemical studies on the iron-only H_2ase from *D. desulfuricans*, bias from H_2-cleavage to -production at pH values of <6 and the interconversion between two states of the oxidized enzyme with different activation properties with an apparent p*K* of 5.9 has been observed,[83] supporting the importance of protonation steps in activation and H_2 formation.

In the iron-only H_2ases, the $[2Fe]_H$ unit of the hydrogen cluster is bound to the protein only via the cysteine link to the [4Fe-4S] cluster and by a few hydrogen bonds.[6−9] Hence, structural flexibility of the $[2Fe]_H$ unit is anticipated. In line with this conjecture, the recent crystal structures reveal pronounced structural differences. In particular, the CO in a semibridging position between the iron atoms in the putatively oxidized iron-only H_2ase[6] appears to be terminally bound to Fe_b (part A of Figure 1) in the reduced enzyme,[7] so that the Fe−Fe bond may be more accessible. It has been postulated that first, reduction and/or hydride binding makes Fe_b (part A of Figure 1) more electron-rich, and, then, the CO moves from the bridging to the terminal position.[7,9] However, the extremely high turnover rate of iron-only H_2-

(81) Schwartz, L.; Ekström, J.; Lomoth, R.; Ott, S. Dynamic Ligation at the First Amine-Coordinated Iron Hydrogenase Active-Site Mimic. *Chem. Commun.* **2006**, 4206−4208.
(82) Zampella, G.; Bruschi, M.; Fantucci, P.; De Gioia, L. DFT Investigation of H_2 Activation by [M(NHPnPr$_3$)(′S3′)] (M = Ni, Pd). Insight into Key Factors Relevant to the Design of Hydrogenase Functional Models. *J. Am. Chem. Soc.* **2005**, *127*, 13180−13189.
(83) Parkin, A.; Cavazza, C.; Fontecilla-Camps, J. C.; Armstrong, F. A. Electrochemical Investigations of the Interconversions between Catalytic and Inhibited States of the [FeFe]-Hydrogenase from *Desulfovibrio desulfuricans*. *J. Am. Chem. Soc.* **2006**, *128*, 16808−16815.

ases seems to be incompatible with such major structural changes at the active site during catalysis. As opposed to the above view, the Fe−Fe site containing a bridging CO may be the one that is active in H_2 cleavage, whereas the site where the CO is in a terminal position is committed to H_2 production, as proposed by M. Darensbourg and coworkers.[30]

The results in the present investigation may support the latter view. In the iron-only hydrogenases, in the presence of protons (at acidic pH values), first a protonation at the adt may occur, leading to a structural change of the Fe−Fe site and to the rotation of the bridging CO to its terminal binding position. Thereby, the ready catalyst ("entatic state"[30]) is generated. Subsequent H^+ binding, reduction of the $[2Fe]_H$ unit by electrons from the attached [4Fe-4S] cluster, and H_2 formation could be concerted and structurally conservative, so that high turnover is achieved.

In the related Ni−Fe H_2ases, H_2 catalysis has been shown to involve a bridging hydride, at least in those enzymes that are sensitive to O_2 inhibition.[22,23] However, such a species may not be involved in H_2 turnover, for example, in the O_2-tolerant NAD^+-reducing hydrogenase from the bacterium *Ralstonia eutropha*, where hydride binding presumably is restricted to the nickel.[51,85] The involvement of a bridging hydride in the iron-only H_2ases is unsettled (above). To clarify this issue, further investigations both on the enzymes and on tailored model compounds are required.

Acknowledgment. M.H. gratefully acknowledges funding by the Deutsche Forschungsgemeinschaft (SFB498, project C8) and the Bundesministerium für Bildung and Forschung (Consortium "Grundlagen für einen biomimetischen and biotechnologischen Ansatz der Wasserstoffproduktion", Grant 035F0318C) and support by Prof. H. Dau (FU-Berlin). We thank the staff at beamline D2 at EMBL (DESY, Hamburg), in particular Dr. W. Meyer-Klaucke and Dr. F. Schäfers and M. Mertin at beamline KMC-1 at BESSY (Berlin) for excellent support. M.S. is grateful to the Klaus Tschira Foundation and the BMBF (Grant 0313076) for financial support and to Drs. L. de Gioia and G. Zampella (University of Milano-Bicocca, Italy) for inspiring discussions; Dr. R.C. Wade is acknowledged for continuous support. S.O. thanks Dr. R. Lomoth (Uppsala University) for valuable discussions; and the Swedish Energy Agency, the Knut and Alice Wallenberg Foundation, the Swedish Research Council and NEST-STRP: SOLAR-H (EU contract nr. 516510) for funding.

Supporting Information Available: Carbonyl region IR-spectra of XAS samples of **1**. This material is available free of charge via the Internet at http://pubs.acs.org.

IC701255P

(84) Stein, M.; Lubitz, W. DFT Calculations of the Electronic Structure of the Paramagnetic States Ni-A, Ni-B and Ni-C of [NiFe] Hydrogenase. *Phys. Chem. Chem. Phys.* **2001**, *13*, 2668−2675.

(85) Van der Linden, E.; Burgdorf, T.; Bernhard, M.; Bleijlevens, B.; Friedrich, B.; Albracht, S. P. The Soluble [NiFe]-Hydrogenase from *Ralstonia eutropha* Contains Four Cyanides in Its Active Site, One of Which is Responsible for the Insensitivity Towards Oxygen. *J. Biol. Inorg. Chem.* **2004**, *9*, 616−626.

(86) Mejia-Rodriguez, M. Ligand Effects on Bioinspired Iron Complexes. Ph.D. Thesis, Texas A&M University, U.S.A., available at: http://txspace.tamu.edu/bitstream/1969.1/2504/1/etd-tamu-2004A-CHEM-Mejia-1.pdf, 2004.